Published in final edited form as:
Pancreas. 2008 November ; 37(4): 440–444. doi:10.1097/MPA.0b013e31817c5113.

Magnetic Resonance Imaging Monitors Physiological Changes With Antihedgehog Therapy in Pancreatic Adenocarcinoma Xenograft Model

Alexander R. Guimaraes, MD, PhD[*,†], **Elena Rakhlin, MD**[‡], **Ralph Weissleder, MD, PhD**[*,†], and **Sarah P. Thayer, MD, PhD**[‡]

[*]Department of Radiology, Center for Molecular Imaging Research, Massachusetts General Hospital, Charlestown

[†]Center for Systems Biology, Massachusetts General Hospital, Boston, MA

[‡]Department of Surgery, Massachusetts General Hospital, Boston, MA

Abstract

Objectives—The sonic hedgehog (Shh) pathway has an established role in pancreatic cancer (pancreatic adenocarcinoma [PDAC]). We tested whether magnetic resonance imaging measures of vascular volume fraction (VVF) using magnetic iron oxide nanoparticles are sensitive to the antiangiogenic effect of targeted Shh therapies in a PDAC xenograft model.

Methods—Pancreatic adenocarcinoma xenograft lines were subcutaneously implanted into nude mice (n = 19 samples within 4 groups). Therapies were targeted to 3 loci of the Shh signaling pathway (anti-Shh antibody, cyclopamine, or forskolin). Magnetic resonance imaging (4.7-T Bruker Pharmascan) was performed (after 1 week of intraperitoneal therapy) before and after intravenous injection of MION-47. Vascular volume fraction was quantified as ΔR2 (from multicontrast T2 sequences) and normalized to an assumed VVF in muscle of 3%. Linear regression compared VVF to histological indices including microvessel density (MVD), viable gland density (VGD), and proliferative index (PI).

Results—In response to anti-Hh treatment, tumors showed a decrease in VGD, PI, MVD, and VVF compared with controls ($P < 0.001$). Vascular volume fraction was compared with histological indicators of response: PI ($R^2 = 0.88$; $P < 0.05$), VGD ($R^2 = 0.87$; $P < 0.05$), and MVD ($R^2 = 0.85$; $P < 0.05$).

Conclusions—Magnetic resonance imaging VVF using magnetic iron oxide nanoparticles may serve as a noninvasive measure of biological response to Shh PDAC therapy with easy translation to the clinic.

Keywords

angiogenesis; magnetic resonance imaging; nanoparticle; pancreatic cancer; sonic hedgehog

In the United States, pancreatic cancer is the fourth most common cause of death from cancer in both men and women.[1,2] Most of the 37,170 new cases diagnosed in 2006, approximately 33,370 will die from their disease. The mortality rates for this disease are higher than those for any other type of cancer.[1,3] Surgical resection of localized disease

Reprints: Alexander R. Guimaraes, MD, PhD, Division of Abdominal Imaging, Department of Radiology, Center for Molecular Imaging Research, Massachusetts General Hospital, White 270, 55 Fruit St, Boston, MA 02114 (aguimaraesl@partners.org)..

offers the only chance for cure of pancreatic cancer. Unfortunately, resection with curative intent is possible in only 10% to 15% of patients presenting with this disease, with a median postoperative survival of only 7 to 13 months and 5-year survival rates of 15% or less.[4,5] Although advances in surgical care have substantially lowered the mortality rate after surgery for pancreatic cancer, these major operations still carry a morbidity rate of 25% to 35%,[6] with approximately 40% of these patients presenting with recurrent disease within 3 years,[1,3] The reasons for this unfortunate outcome include poor diagnostic capabilities at the early stage of the disease,[7–9] which is likely a causality of the insidious nature of the disease with a lack of specific symptoms; early occurrence of metastatic disease; and a poor understanding of the etiology of pancreatic cancer.[7–9] By the time of diagnosis, metastatic disease to the peritoneum, liver, or regional lymph nodes occurs in up to 80% of patients.[1,7] Treatment options for this population of patients remain limited.

The causes of pancreatic cancer are not yet well understood.[1,7,8,10] Many factors contribute to the aggressive growth, survival, and metastasis of pancreatic cancer including the up-regulation or activation of mitogenic signals, growth factors, and their receptors in addition to numerous oncogenic genes (ie, epidermal growth factor, K-*ras*, Src, and sonic hedgehog [Shh]) concomitant with the down-regulation of tumor suppressor genes (ie, p53 and PTEN) may all contribute to the early and late stages of pancreatic carcinogenesis.[7,8,10–19] The hedgehog developmental signaling pathway has been implicated in the development of pancreatic cancer.[20,21] The up-regulated expression of the Shh ligands in pancreatic cancer cells seems to result in the depression of smoothen (Smo), part of the Hh receptor complex, which ultimately activates the transcriptional factor, Gli, resulting in increased expression of a multitude of oncogenic genes involved in the progression of this disease.[8,20–24] Recent findings demonstrate that Shh expression enhances pancreatic tumor initiation and growth while reducing tumor cell death after therapy, all of which demonstrate the role of Shh signaling in pancreatic tumor initiation, growth, and survival.[25] These data suggest that targeted therapies may provide a novel therapeutic strategy in pancreatic cancer. Recent results also suggest that Shh potentiates angiogenesis, improves wound healing in diabetic models, and may also play a proangiogenic role in pancreatic cancer.[26,27]

Magnetic resonance imaging (MRI) provides high-spatial resolution noninvasive imaging of soft tissue anatomy with high soft tissue contrast. We have shown in various xenograft murine models that MRI enhanced with intravenously administered long-circulating magnetic nanoparticles (MNPs) provides a noninvasive, accurate, and sensitive assessment of vascular volume fraction (VVF), which is a surrogate marker of microvessel density (MVD), and angiogenesis.[28,29] We postulate that this technology may provide a noninvasive window into the physiological changes associated with targeted Shh therapy. We tested this hypothesis by applying MRI enhanced with MNP to a pancreatic ductal adenocarcinoma cell xenograft model after targeted therapies either to the Shh ligand, Smo (the Hh receptor complex), or the downstream transcriptional activators Gli by using either 5E1 antibody, cyclopamine, or forskolin, respectively. All tumor xenografts in this model were derived from patients' primary and metastatic tumors, whose expression of the Hh pathway was determined by quantitative real-time reverse transcriptase–polymerase chain reaction. By correlating the MRI-derived index VVF to the histological indices MVD, proliferative index (Ki-67), and viable gland index, we investigate the role of MRI for monitoring those physiological changes associated with anti-Shh targeted therapy.

MATERIALS AND METHODS

Animal Model

Human pancreatic adenocarcinoma (PDAC) specimens were collected in accordance with institutional review board regulations. Freshly resected specimens were implanted

subcutaneously into nude mice according to an institutionally approved protocol. Tumors were allowed to reach the size of 125 μL, harvested, and replanted into the second generation of nude mice (MP2). These mice were used for evaluation of targeted antihedgehog therapy. Treatments included 5e1 antibody (Developmental Studies Hybridoma Bank, University of Iowa) 300 mg of SC daily, cyclopamine 0.6 mg IP daily, and forskolin 75 mg IP. Control injections were performed with 150 μL of normal saline, administered subcutaneously. Animals were killed after a 7-day course of treatment; tumors were harvested, preserved in 10% formalin overnight, and embedded in paraffin.

Magnetic Resonance Imaging

Magnetic resonance imaging was performed at 4.7 T on a Bruker imaging system (Pharmascan, Karlsruhe, Germany). Animals were imaged immediately after 1 week of therapy. Animals were anesthetized during imaging with 1% to 1.5% inhaled isofluorane and monitored during imaging with respiratory monitoring. Imaging protocols included a triplane and axial rapid acquisition with relaxation enhancement localizer. Multislice multiecho T2-weighted imaging was performed before and after intravenous injection of MNP (10 mg/kg iron). The following parameters were used: flip angle, 90 degrees; matrix size, 128 × 64; repetition time, 2500 milliseconds; time to echo [TE], 16 equally spaced echoes at 8.6-millisecond intervals ranging from 8.6 to 137 milliseconds; field of view, 4.24 × 2.12 cm; and slice thickness, 1 mm. T1-weighted imaging was performed after the administration of intravenous gadolinium-diethylenetriamine pentaacetic acid using the following parameters: flip angle, 90 degrees; matrix size, 256 × 256; repetition time, 700 milliseconds; TE, 14 milliseconds; field of view, 4.24 × 2.12 cm; slice thickness, 1 mm.

Vascular volume fraction measures were calculated from the precontrast and postcontrast MNP-enhanced images as described in detail elsewhere.[28,30,31] A fundamental assumption is that the change in the transverse relaxation rate ([ΔR2* = 1/ΔT2*] and [ΔR2 = 1/ΔT2]) relative to the preinjection baseline is proportional to the perfused local blood volume per unit tumor volume (V) multiplied by a function (*f*) of the plasma concentration of the agent (P).

$$\Delta \mathrm{R2} = \mathrm{k} \cdot f\,(\mathrm{P}) \cdot \mathrm{V}$$

Assuming a steady state for MNP distribution, the R2 was fit by using a monoexponential fitting algorithm for the multi-TE data (OsiriX). Region of interest incorporating the center 3 to 4 slices of the tumor as well as nearby muscle within the same slices were analyzed before and after MNP administration. ΔR2 was then converted to absolute tumoral VVF by scaling measurements to muscle with a known VVF of 3%. In addition, analysis was performed on a pixel-by-pixel basis to further assess geographic distribution of VVF. Data are reported as VVF ± SEM.

Histology and Immunohistochemistry

Paraffin-embedded tissues were cut in 6-μm sections, and hematoxylin and eosin stains were performed in routine fashion. To determine viable gland density (VGD), pictures of the entire cross-section of the tumor were taken under × 100 magnification. Each picture was evaluated using Metamorph software to determine the number of pixels occupied by viable tumor glands. Total pixels representing the adenocarcinoma component of the tumor were added and expressed as a percentage of the total number of tumor pixels.

Immunohistochemistry for the Ki-67 was performed using a standard protocol. Antigen retrieval was performed in Retrivex pH6 solution using a pressure cooker (InnoGenex, San

Ramon, Calif). Anti-Ki67 antibody (sc-15402; Santa Cruz Biotechnology, Santa Cruz, Calif) is used at 1:100 dilution with an overnight incubation. Biotinylated secondary anti-rabbit antibody (Vector Laboratories, Burlingame, Calif) used at 1:500 dilution was applied for 1 hour. Antigen was visualized using DAB (Zymed; Invitrogen, Carlsbad, Calif) that produced brown pigmentation. Slides were counterstained with hematoxylin and mounted.

Proliferative index was calculated by photographing the entire slide at ×100 magnification. These pictures were analyzed in Metamorph for pixel representing Ki-67 positive nuclei. The final proliferative index value was expressed as a number of Ki67-positive pixels per ×100 field.

To determine MVD, sections were stained with an anti-CD31 antibody (Santa Cruz Biotechnology). Three representative sections per tumor were analyzed. Results are reported as mean vessel number ± SD per ×20 high-power field.

Statistical Analysis

One-way analysis of variance (ANOVA) was performed comparing VVF as determined from n = 3 to 4 slices within the treatment groups (control [n = 6], Ab5E1 [n = 7], cyclopamine [n = 3], and forskolin [n = 3]). As well, linear regression analysis was performed comparing VVF to MVD, Ki-67, and VGD.

RESULTS

VVF Correlates With Histological MVD Measurements

T1-weighted MRI axial images of mice status post xenograft implantation of pancreatic ductal carcinoma in the left thoracic wall and a 3-dimensional volume-rendered image of the mouse thorax and entire tumor (Figs. 1A–D). Superimposed over the tumor is a pseudocolorized VVF map whose voxel color, and color bar on the far left, is representative of the VVF. In all mice, VVF revealed heterogeneous vascularity throughout the tumor. In control mice, a rich network of vessels are identified throughout the tumor (Fig. 1B). Murine xenografts were then treated with antihedgehog agents: Ab5E1, an anti–sonic hedgehog antibody; cyclopamine, directed against Smo, part of the Hh receptor complex; and forskolin, an inhibitor of the Hh downstream transcriptional activator Gli. In response to anti-Hh agents, there was a marked decrease in VVF in treated tumors (Figs. 1C, D) Quantitative analysis using mean VVF also supported the qualitative observations. Mean VVF ± SEM of control tumors were 11.0 ± 0.5 versus 4.0 ± 0.5 for Ab5E1, 4.3 ± 0.6 for forskolin, and 0.7 ± 0.4 for cyclopamine (Table 1). Statistical analysis incorporating ANOVA demonstrated a statistically significant difference ($P < 0.001$) among all these groups. To ascertain if VVF identified by MRI correlated with vascular density, tumors were stained with CD31, an endothelial marker, to determine MVD. In control animals, CD31 staining revealed a rich network of capillaries throughout the tumor (Fig. 1F), which had been predicted by MRI imaging of VVF (Figs. 1A, B). Antihedgehog treatment resulted in a marked decrease in the MVD revealed by the lack of CD31 staining in treated animals (Figs. 1G, H). Least squares linear regression analyses were performed comparing VVF to MVD and demonstrates good correlation $R^2 = 0.85$ ($P < 0.05$). These data demonstrate that MRI measures of VVF can monitor noninvasively the vascular changes associated with therapy in this xenograft model.

MRI Using VVF May Be Able to Predict Biological Response to Treatment

Magnetic resonance imaging VVF was correlated with other histological measures including Ki-67 (proliferative index) and viable gland index. Anti-Hh treatment resulted in a reduction in proliferation and viable glands throughout the tumor (Figs. 2A–H). Histological analyses

of Ki-67 and viable gland index representing mice treated with sonic hedgehog antibody, cyclopamine, and forskolin resulted in a decrease in staining relative to control vehicle (Figs. 2A–H). Least squares analysis of VVF versus Ki-67 (proliferative index), and viable gland index, revealed an excellent correlation (R^2 = 0.88 and 0.87, respectively [$P < 0.05$]) among these groups. Of note, the correlation of MVD versus Ki-67 and viable gland index were 0.58 and 0.61, respectively (data not shown). In summary, these data suggest that VVF may also be a good indicator of biological response.

DISCUSSION

Magnetic resonance imaging provides high–spatial resolution noninvasive imaging of anatomy with high soft tissue contrast. We have shown in various xenograft murine models that MRI enhanced with intravenously administered long-circulating MNPs provides a noninvasive, accurate, and sensitive assessment of VVF, which is a surrogate marker of MVD, and angiogenesis.[28,29] We postulate that this technology may provide a noninvasive window into the physiological changes associated with targeted Shh therapy. We tested this hypothesis by applying MRI enhanced with MNP to a pancreatic ductal adenocarcinoma cell xenograft model after targeted therapies against different components of the Hh pathway.

Our results demonstrate that MRI measures of VVF quantify changes after targeted therapies. Magnetic resonance imaging VVF correlates highly to histopathologic indices of MVD and may serve as a surrogate marker of angiogenesis confirming previous results.[28,29] Furthermore, we found high correlation of MRI VVF to other histological indices (viable gland index and proliferative index) subtly associated with treatment. These results suggest that MRI VVF may serve as an early predictive marker of therapeutic efficacy.

Acknowledgments

The authors thank Denise Long for help in xenograft model development, animal care, animal treatment, and data analysis. As well, the authors thank Peter Waterman, Carlos Rangel, and Claire Kaufman for assistance in magnetic resonance imaging data gathering.

This study was supported by Dr Thayer's Lustgarten Foundation and K08–Mentored Clinical Scientist Development Award (S.P.T.).

REFERENCES

1. Greenlee RT, Murray T, Bolden S, et al. Cancer statistics. CA Cancer J Clin. 2000; 50:7–33. [PubMed: 10735013]
2. Lim JE, Chien MW, Earle CC. Prognostic factors following curative resection for pancreatic adenocarcinoma: a population-based, linked database analysis of 396 patients. Ann Surg. 2003; 237(1):74–85. [PubMed: 12496533]
3. Lim JE, Chein MW, Earle CC. Prognostic factors following curative resection for pancreatic adenocarcinoma. Ann Surg. 2003; 238(1):74–85. [PubMed: 12496533]
4. Geer RJ, Brennan MF. Prognostic indicators for survival after resection of pancreatic adenocarcinoma. Am J Surg. 1993; 165:68–72. [PubMed: 8380315]
5. Sener SF, Fremgen A, Menck HR, et al. Pancreatic cancer: a report of treatment and survival trends for 100,313 patients diagnosed from 1985–1995, using the National Cancer Database (see comments). J Am Coll Surg. 1999; 189:1–7. [PubMed: 10401733]
6. Yeo CJ, Cameron JL, Sohn TA, et al. Pancreaticoduodenectomy with or without extended retroperitoneal lymphadenectomy for periampullary adenocarcinoma: comparison of morbidity and mortality and short-term outcome. Ann Surg. 1999; 229(5):613–631. [PubMed: 10235519]
7. Li D, Xie K, Wolff R, et al. Pancreatic cancer. Lancet. 2004; 363(9414):1049–1057. [PubMed: 15051286]

8. Mimeault M, Brand RE, Sasson AA, et al. Recent advances on the molecular mechanisms involved in pancreatic cancer progression and therapies. Pancreas. 2005; 31(4):301–316. [PubMed: 16258363]
9. Postier RG. The challenge of pancreatic cancer. Am J Surg. 2003; 186(6):579–582. [PubMed: 14672761]
10. Bardeesy N, DePinho RA. Pancreatic cancer biology and genetics. Nat Rev Cancer. 2002; 2(12): 897–909. [PubMed: 12459728]
11. Friess H, Ding J, Kleeff J, et al. Microarray-based identification of differentially expressed growth- and metastasis-associated genes in pancreatic cancer. Cell Mol Life Sci. 2003; 60(6):1180–1199. [PubMed: 12861384]
12. Holzmann K, Kohlhammer H, Schwaenen C, et al. Genomic DNA-chip hybridization reveals a higher incidence of genomic amplifications in pancreatic cancer than conventional comparative genomic hybridization and leads to the identification of novel candidate genes. Cancer Res. 2004; 64(13):4428–4433. [PubMed: 15231651]
13. Joyce JA, Laakkonen P, Bernasconi M, et al. Stage-specific vascular markers revealed by phage display in a mouse model of pancreatic islet tumorigenesis. Cancer Cell. 2003; 4(5):393–403. [PubMed: 14667506]
14. Missiaglia E, Blaveri E, Terris B, et al. Analysis of gene expression in cancer cell lines identifies candidate markers for pancreatic tumorigenesis and metastasis. Int J Cancer. 2004; 112(1):100–112. [PubMed: 15305381]
15. Ohno K, Hata F, Nishimori H, et al. Metastatic-associated biological properties and differential gene expression profiles in established highly liver and peritoneal metastatic cell lines of human pancreatic cancer. J Exp Clin Cancer Res. 2003; 22(4):623–631. [PubMed: 15053306]
16. Saad ED, Hoff PM. Molecular-targeted agents in pancreatic cancer. Cancer Control. 2004; 11(1): 32–38. [PubMed: 14749621]
17. Sakorafas GH, Tsiotou AG, Tsiotos GG. Molecular biology of pancreatic cancer; oncogenes, tumour suppressor genes, growth factors, and their receptors from a clinical perspective. Cancer Treat Rev. 2000; 26(1):29–52. [PubMed: 10660490]
18. Shi X, Liu S, Kleeff J, et al. Acquired resistance of pancreatic cancer cells towards 5-fluorouracil and gemcitabine is associated with altered expression of apoptosis-regulating genes. Oncology. 2002; 62(4):354–362. [PubMed: 12138244]
19. Trauzold A, Schmiedel S, Oestern S, et al. Concerted deregulations of multiple apoptosis-controlling genes in pancreatic carcinoma cells. Ann N Y Acad Sci. 2003; 1010:510–513. [PubMed: 15033781]
20. Thayer S. The emerging role of the hedgehog signaling pathway in gastrointestinal cancers. Clin Adv Hematol Oncol. 2004; 2(1):17–63. [PubMed: 16163153]
21. Thayer SP, di Magliano MP, Heiser PW, et al. Hedgehog is an early and late mediator of pancreatic cancer tumorigenesis. Nature. 2003; 425(6960):851–856. [PubMed: 14520413]
22. Kayed H, Kleeff J, Keleg S, et al. Indian hedgehog signaling pathway: expression and regulation in pancreatic cancer. Int J Cancer. 2004; 110(5):668–676. [PubMed: 15146555]
23. Kayed H, Kleeff J, Osman T, et al. Hedgehog signaling in the normal and diseased pancreas. Pancreas. 2006; 32(2):119–129. [PubMed: 16552330]
24. Xie K, Abbruzzese JL. Developmental biology informs cancer: the emerging role of the hedgehog signaling pathway in upper gastrointestinal cancers. Cancer Cell. 2003; 4(4):245–247. [PubMed: 14585350]
25. Morton JP, Mongeau ME, Klimstra DS, et al. Sonic hedgehog acts at multiple stages during pancreatic tumorigenesis. Proc Natl Acad Sci U S A. 2007; 104(12):5103–5108. [PubMed: 17372229]
26. Asai J, Takenaka H, Kusano KF, et al. Topical sonic hedgehog gene therapy accelerates wound healing in diabetes by enhancing endothelial progenitor cell-mediated microvascular remodeling. Circulation. 2006; 113(20):2413–2424. [PubMed: 16702471]
27. Donahue JK. Gene therapy, angiogenesis, Sonic Hedgehog: Sonic the Hedgehog to the rescue? Gene Ther. 2006; 13(13):998–999. [PubMed: 17262905]

28. Bremer C, Mustafa M, Bogdanov A Jr, et al. Steady-state blood volume measurements in Experimental tumors with different angiogenic burdens—a study in mice. Radiology. 2003; 226(1):214–220. [PubMed: 12511693]

29. Tang Y, Kim M, Carrasco D, et al. In vivo assessment of RAS-dependent maintenance of tumor angiogenesis by real-time magnetic resonance imaging. Cancer Res. 2005; 65(18):8324–8330. [PubMed: 16166309]

30. Boxerman J, Hamberg L, Rosen B, et al. MR contrast due to intravascular magnetic susceptibility perturbations. Magn Reson Med. 1995; 34:555–566. [PubMed: 8524024]

31. Dennie J, Mandeville J, Boxerman J, et al. NMR imaging of changes in vascular morphology due to tumor angiogenesis. Magn Reson Med. 1998; 40:793–799. [PubMed: 9840821]

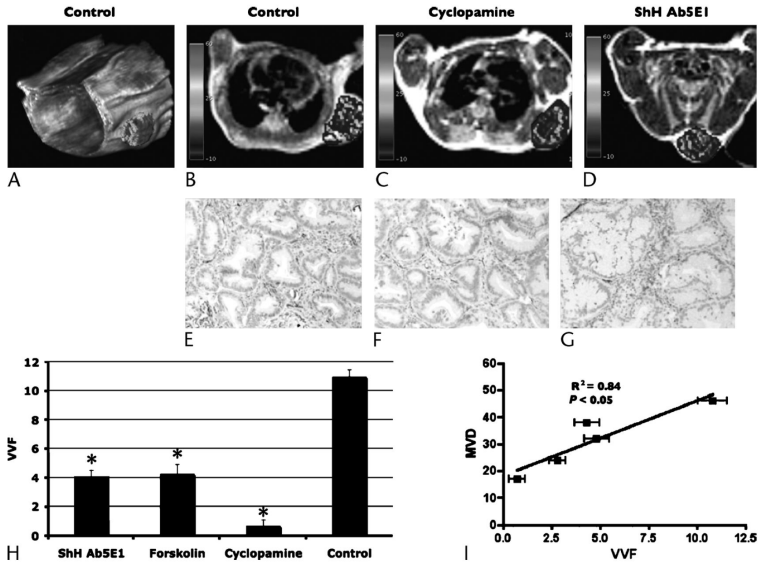

FIGURE 1.

Magnetic resonance imaging enhanced with MNPs demonstrating the VVF of xenograft tumors in mice with high correlation to histological measures of MVD. A, Three-dimensional volume-rendered image of a control mouse that demonstrates over the right flank, a xenograft tumor with VVF with pseudocolorized 3-dimensional VVF superimposed. B–D, T1-weighted axial MRI images of mice status post xenograft implantation of pancreatic ductal carcinoma in the left thoracic wall. Superimposed over the tumor is a pseudocolorized map of VVF with color bar on the left correlating to VVF within the tumor. C and D, There is decreased vascularity in VVF in those mice treated with cyclopamine and Ab5E1 as compared with control. E–G, In control animals, CD31 staining revealed a rich network of capillaries throughout the tumor. F and G, Antihedgehog treatment resulted in a marked decrease in the MVD revealed by the lack of CD31 staining in cyclopamine- (F) and Ab5E1-treated (G) animals. H, Quantitative analysis using mean VVF also supported the qualitative observations. Mean VVF ± SEM of control tumors are 11.0 ± 0.5 versus 4.0 ± 0.5 for Ab5E1, 4.3 ± 0.6 for forskolin, and 0.7 ± 0.4 for cyclopamine (Table 1). Statistical analysis (ANOVA) demonstrated a statistically significant difference ($P < 0.001$) among all these groups. I, Least squares linear regression analyses were performed comparing VVF with MVD and demonstrates excellent correlation, $R^2 = 0.85$ ($P < 0.05$).

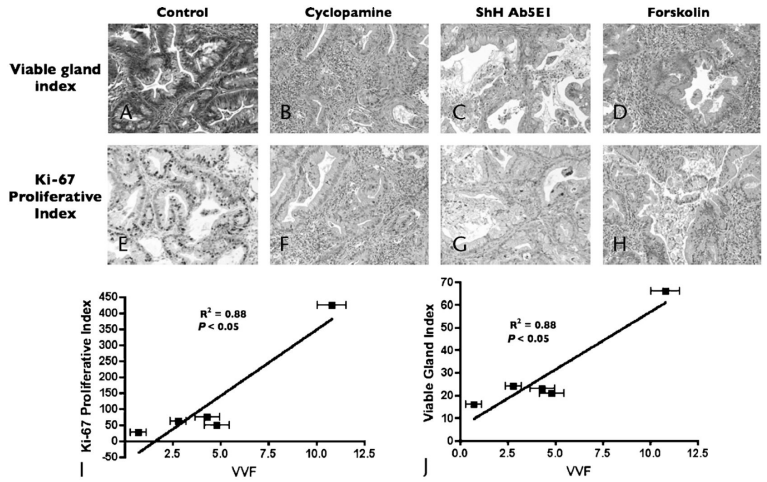

FIGURE 2.

Magnetic resonance imaging VVF was correlated to other histological measures including Ki-67 (proliferative index) and viable gland index (VGD). A–D, Histological analysis demonstrated increased areas of confluent necrosis with increased glandular component, resulting in decreased viable gland index in cyclopamine- (B), Ab5E1- (C), and forskolin-treated (D) animals relative to control (A). E–H, Histological analysis for proliferative index demonstrated a decreased proportion of Ki-67–positive cells in cyclopamine- (F), Ab5E1- (G), and forskolin-treated (H) animals relative to control (E). I and J, Least squares analysis of VVF versus Ki-67 (proliferative index) (I), and viable gland index (J), revealed an excellent correlation (R^2 = 0.88 and 0.88, respectively; [$P < 0.05$]) among these groups.

Table 1

Data Summary

Mouse	VVF	MVD	Ki-67	Viable Gland Index
Shh Ab5E1	4.8	32	50	21
Shh Ab5E1	2.8	24	62	24
Forskolin	4.3	38	75	23
Cyclopamine	0.7	17	27	16
Control	11	46	425	66

Data summary for mice in each treatment cohort (column 1). Data in each column are as follows: vascular volume fraction (VVF) (column 2, expressed in %), micro vessel density (MVD) (column 3, expressed as mean vessel number), Ki-67 proliferative index (column 4, expressed as Ki-67 positive pixels per × 100 field); and viable gland index (column 5, expressed as percentage of total number of viable tumor cells relative to tumor pixels).